# Direct Observation of Interfacial Charge Recombination to the Excited-Triplet State in All-*trans*-Retinoic Acid Sensitized $TiO_2$ Nanoparticles by Femtosecond Time-Resolved Difference Absorption Spectroscopy

**Lei Zhang, Jian Yang, Li Wang, Guo-Zhen Yang, and Yu-Xiang Weng***

*Institute of Physics, Chinese Academy of Sciences, Beijing 100080, China*

*Received: May 7, 2003; In Final Form: September 23, 2003*

The excited-state dynamics of all-*trans*-retinoic acid (ATRA), both free in *n*-hexanol and bound to a $TiO_2$ nanoparticle have been studied by use of femtosecond time-resolved visible absorption spectroscopy excited at 400 nm. Three excited singlet states, $S_3$, $S_2$, and $S_1$, have been observed for the ATRA molecule, which can be assigned as $1B_u^+$ ($\pi$, $\pi^*$), (n, $\pi^*$), and $2A_g^-$ ($\pi$, $\pi^*$) singlet excited manifolds, respectively. Photoinduced electron injection from the excited singlet state $S_3$ to the conduction band of the $TiO_2$ nanoparticle is observed in an ATRA-sensitized $TiO_2$ colloidal solution in hexanol; the subsequent interfacial charge recombination between the injected electron and the ATRA cation is investigated. It is found that the charge recombination is mainly via the triplet state, and the branching ratio for the population on the excited triplet state and the ground state during the charge recombination is about 6.0. The observed rate constants for the charge recombination to the triplet state and the ground state are 1/19.0 ($ps^{-1}$) and 1/140 ($ps^{-1}$), respectively. Treating the charge recombination as a nonadiabatic process, we can obtain a reorganization energy having a value of 0.44 eV, which indicates that the charge recombination to the ground state is in the Marcus inverted region while the charge recombination to the triplet state lies within the normal region. An apparent electronic coupling matrix element at the closest contact of ATRA and the $TiO_2$ nanoparticle, $V_0^T = 5118\ cm^{-1}$, has been evaluated for the charge recombination to the triplet state and $V_0^G = 2670\ cm^{-1}$ for that to the ground state. It is concluded that the interfacial charge recombination is strongly coupled. The electronic coupling matrix element is expected to decay exponentially on the charge separation distance, and in the microsecond domain, the observed $V(r)^G$ decays to 3.6 $cm^{-1}$, corresponding to the trapped electron migrating away from the adsorbates at a distance of 2.0 nm on the $TiO_2$ nanoparticles. The relevance of the triplet formation to the electroluminescence device is also discussed.

## Introduction

Charge recombination to the triplet state has attracted intensive interest because of its importance in the natural photosynthetic process,[1−6] electroluminescence in manufacturing display devices,[7−9] and potentially applicable mesoporous dye-sensitized $TiO_2$ nanocrystalline solar cells.[10,11]

In photosynthesis, an appreciable amount of triplet chlorophylls (Chl) can be generated during the light-driven primary electron-transfer reactions, which occurs with a quantum yield of 4.5% in plant.[12,13] The triplet chlorophyll is energetic enough to react with the triplet oxygen (ground state) to form singlet oxygen, which can attack organisms. It has been shown that all of the wild-type photosynthetic organisms are equipped with a photoprotection mechanism by using the triplet state of carotenoids ($^3$Car) as the "triplet valves" for the excess energy dissipation.[12] This function can be realized in two ways, by either a destructive reaction of Car with singlet oxygen or a more important nondestructive triplet energy transfer process with $^3$Chl to prevent the formation of the singlet oxygen. In the latter case, Car becomes $^3$Car after accepting energy from $^3$Chl, while $^3$Car cannot react with the ground-state oxygen to form the singlet oxygen;[14] instead it dissipates the excess energy by a harmless nonradiative decay to the ground state. It is generally accepted that $^3$Chl is derived mainly from the intersystem crossing within the singlet-born radical ion pair. The intersystem crossing from the singlet radical ion pair leads to the generation of the triplet radical ion pair, and the $^3$Chl is formed upon the charge recombination within the triplet precursor of the radical ion pair. It has been proposed that the intersystem crossing from the singlet radical ion pair to the triplet ion pair is through a $S-T_0$ mixing by Zeeman and hyperfine interaction mechanism, which is a relatively slow process and can be at a time scale of several nanoseconds or longer,[15,16] suitable for time-resolved electron paramagnetic spin resonance (EPR) study. Mimicking of the triplet generation in photosynthesis has been successful in a number of triad supermolecular systems with a D−A (donor−acceptor) distance larger than 20 Å. In these cases, the photogenerated radical ion pairs are weakly coupled having a small exchange integral.[17,18] In a strongly coupled covalently linked D−A system with a smaller separation (11 Å), charge recombination to the triplet states has also been observed, and the generation of the triplet state is attributed to the strongly coupled singlet radical ion pairs that undergo intersystem crossing to form the triplet precursor through $S-T_0$ and $S-T_{-1}$ mixing.[19] In such a strongly coupled system, the charge recombination within the triplet radical ion pairs is much faster than that of the weakly coupled system with a decay constant of several to several tens of nanoseconds.[19, 20]

It has been shown that charge recombination to the triplet states is affected by a number of factors such as configuration

* To whom correspondence should be addressed. E-mail: yxweng@aphy.iphy.ac.cn. Phone: +86-10-82649342. Fax: +86-10-82649451.

10.1021/jp035236e CCC: $25.00 
Published on Web 11/12/2003

**SCHEME 1: Schematic Diagram for All-*trans*-retinoic Acid Bound to $TiO_2$ Nanoparticle[a]**

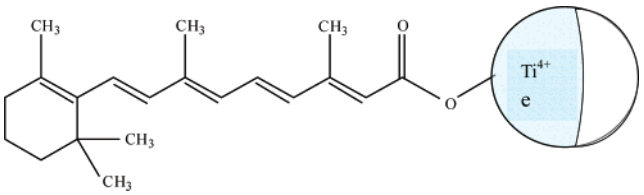


[a] The shaded area of the $TiO_2$ nanoparticle represents the distribution area of the injected electron trapped on the surface.

of the D−A pair,[16] D−A separation,[18,19] solvent,[21] driving forces, external magnetic field,[22] and paramagnetic molecules.[15] Among these factors, the effect of driving force is less explored. It has been proposed that in a carotene−porphyrin−fullerene triad system, when the driving force of the charge recombination to the ground state falls in the Marcus inverted region, charge recombination to the ground state is much more inverted with respect to that to the triplet state, which leads to the charge recombination path via the excited triplet state being kinetically favored.[16] However, direct observation of such a fast electron recombination to the triplet state induced by driving force has been scarcely reported. The reason is twofold: first if such a process is fast enough to compete with the spin−orbital intersystem crossing, it may not be easy to differentiate whether the triplet state comes from the intersystem crossing or back electron transfer; second if this process is within a nanosecond or longer time domain, it overlaps temporally with the radical pair intersystem crossing (RP-ISC) process. In our recent nanosecond flash photolysis study of all-*trans*-retinoic acid (ATRA) assembled onto the $TiO_2$ nanoparticle (ATRA−$TiO_2$, see Scheme 1), we found that a substantial amount of $ATRA^T$ (ATRA triplet state) has been formed after laser excitation, which cannot be accounted by the mechanism of intersystem crossing from the ATRA excited singlet state. We proposed that the triplet state arises from the interfacial charge recombination between the trapped electron and $ATRA^+$ (ATRA radical cation). The account for such a charge recombination to the triplet state is given as the charge recombination between the trapped electron and $ATRA^+$ to the ground state being expected to be in the Marcus inverted region, giving rise to the charge recombination to the triplet state being kinetically favored.[23,24] However, experimental confirmation of the population of ATRA triplet state from the charge recombination in a shorter time scale remains to be performed. We have noted that in a recent paper and in a quite similar system, that is, 8-apo-8′-carotenoid acid sensitized $TiO_2$ nanoparticle, direct charge recombination between the trapped electron and the carotenoid acid cation to the triplet state has been observed in a picosecond domain.[25]

In the present work, we report our continued study of interfacial electron transfer in the ATRA−$TiO_2$ colloidal solution with femtosecond time-resolved transient absorption spectroscopy. The photophysics of the ATRA molecule is explored. Efforts have been made to distinguish whether the excited-triplet-state generation is from the spin−orbital intersystem crossing or charge recombination, and the population of excited-triplet-state ATRA from the charge recombination is confirmed unambiguously. An interesting point for such interfacial charge recombination between the trapped electron on the semiconductor surface and the radical cation of the dye is that the initial spin correlation for the injected electron would be completely lost during the relaxation of the injected electron within the conduction band, unlike those in the photosynthetic systems and the artificial mimicking supermolecular systems where the initial radical−electron pairs have a singlet spin because of the optically allowed transition; the charge recombination in the present system is more like the exciton (electron−hole) recombination within the organic polymer in the electroluminescence (EL) process where the charge recombination is also spin-uncorrelated. Therefore study of such an interfacial spin-uncorrelated charge recombination process would shed light into the EL process.

## Experimental Section

**Materials.** All-*trans*-retinoic acid (Aldrich), titanium(IV) *n*-butoxide (99%) (ACROS), solvents, and other reagents were analytical grade used without further purification.

The $TiO_2$ colloidal solution was prepared by hydrolysis of titanium(IV) *n*-butoxide in a hexanol/$H_2O$ mixture. An amount of 0.08 g of titanium(IV) *n*-butoxide was added into 10 mL of hexanol and stirred for complete mixing under a $N_2$ gas stream. An aliquot of 1 mL of $H_2O$ with pH preadjusted to 2.0 was added to 30 mL of hexanol and sonicated for complete mixing. The $H_2O$/hexanol mixture was cooled in an ice/water bath and kept stirring; then titanium(IV) *n*-butoxide dissolved in hexanol was added dropwise under a $N_2$ gas stream. After the completion of the reaction, a clear colloidal solution was obtained. The solvent was evaporated by rotary evaporator at room temperature, and the powdered $TiO_2$ sample was obtained. X-ray diffraction measurement of the powdered sample showed that it consists of mainly amorphous $TiO_2$ and possibly a brookite phase with an average size of ca.1.4 nm in diameter estimated by the well-known Sherrer equation. Transmission electron micrograph (TEM) selected electron diffraction patterns showed that $TiO_2$ nanoparticles are polycrystalline. Combining the results of both XRD measurement and electron diffraction analysis, we tentatively conclude that the $TiO_2$ nanoparticles prepared in hexanol contain mainly amorphous-like $TiO_2$ with a possible presence of brookite phase.

The ATRA−$TiO_2$ colloidal solution was prepared by addition of a concentrated ATRA−methanol solution ($c = 2 \times 10^{-3}$ M) into the $TiO_2$ colloidal solution and stirring for 3 h in the dark under an Ar stream for dye-sensitization, keeping the apparent ATRA concentration in the bulk at $2 \times 10^{-5}$ M.

**Measurements.** The femtosecond time-resolved absorbance difference spectrometer employs a regenerative Ti:sapphire amplifier laser with 1 kHz repetition (Hurricane, Spectra Physics) as the primary laser source. The output power of the laser is 750 mJ with a pulse duration of 150 fs (full width at half-measure, fwhm) at 800 nm. The output beam was split into two. One with a power of 6 $\mu$J/pulse is focused onto a flowing cell filled with $H_2O$ at an optical path length of 2 mm to generate a white light continuum as a probe beam. The white light continuum covers a spectral region from about 420 to 900 nm. Another beam was frequency doubled after passing a translation stage and used as a pump beam. A dual beam configuration (signal and reference) was adopted for the detection. The signal and reference beams were collected by a pair of objective lenses coupled to a two-branched optical fiber coupled to a CCD spectrometer (Acton). The delay between pump and probe beam was realized by a computer-controlled translation stage. The polarization of the 400 nm pump beam was set to the magic angle (54.7°) with respect to the probe beam.

Because polyenes are labile to the photoinduced isomerization, circulation of a large amount of sample would prevent the interference from the accumulation of the side products. Thus 200 mL of sample solution was used in a flowing cell for the time-resolved spectroscopic measurement. UV−visible absorp-

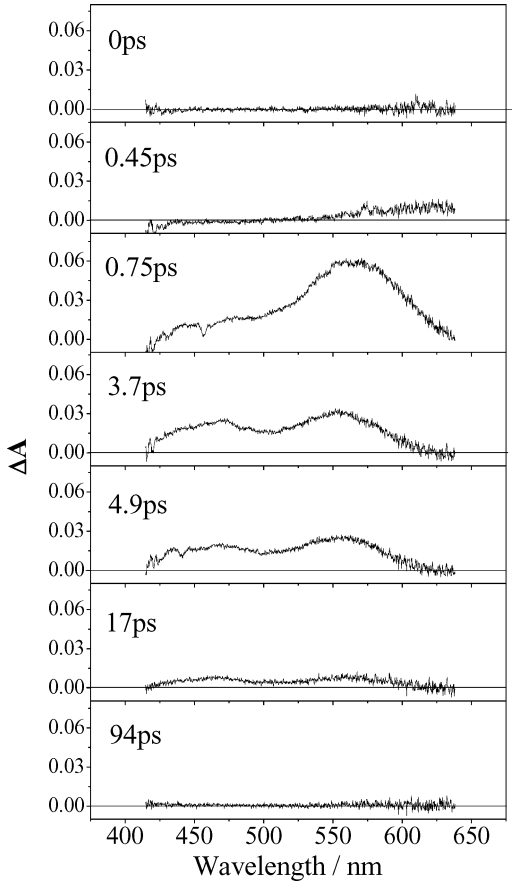


**Figure 1.** Seven chirp-corrected time-resolved absorbance difference spectra of free ATRA in hexanol purged with Ar gas excited at 400 nm, 5 $\mu$J/pulse.

tion spectra before and after the experiments showed almost no change.

## Results

**Femtosecond Time-Resolved Difference Absorption Spectra of Free ATRA.** Retinyl chromophore has a special importance in biology. It is a key chromorphore found in the opsin as a retinal Schiff base. It acts as a photon receptor and photoelectrosignal generator via photoinduced cis−trans isomerization and the successive proton transfer.[26,27] It has five C═C double bonds in its polyenic backbone, a structural analogue of carotenoids with a fewer number of conjugated C═C double bonds. To assemble the retinyl moiety to the $TiO_2$ surface, a carboxylic group was employed to serve as an interfacial anchor.[28,29]

Figure 1 shows seven chirp-corrected time-resolved absorbance difference spectra of free ATRA in hexanol purged with Ar gas excited at 400 nm. The transient absorbance signal is caused by transitions from the excited states to the corresponding optically allowed higher excited states. A sharp minus peak at 457 nm has a temporal evolution profile similar to the cross-correlation profile of the laser pulse, which is 3118 $cm^{-1}$ red-shifted with respect to the excitation laser, and this can be assigned as the impulsive stimulated Raman gain signal from the CH stretching modes of the solvent hexanol.[30]

As shown in Figure 1, the absorption peak around 600 nm rises in the early time and then comes up with a gradual rising of the absorbance at 558 nm and then 446 nm. Obviously, there are several excited states that have been populated after the photoexcitation. After 90 ps, almost all of the observable excited states decay completely, which also indicates that no observable amount of excited triplet state is formed from the intersystem crossing. This is in agreement with the fact that no transient signal from the triplet state is detected in the submicrosecond time domain when ATRA is excited at 355 nm in various solvents.[23,24] The lifetime and corresponding component spectra can be resolved by the single value decomposition (SVD) method together with global fittings.[30−32] The result of the SVD analysis is displayed in Figure 2, which shows that there are three principal singular values, 8.2746, 1.2816, and 0.5958. The fourth one is 0.3154, and higher-order singular values are smaller than 0.2533, and their contributions are regarded as noise.

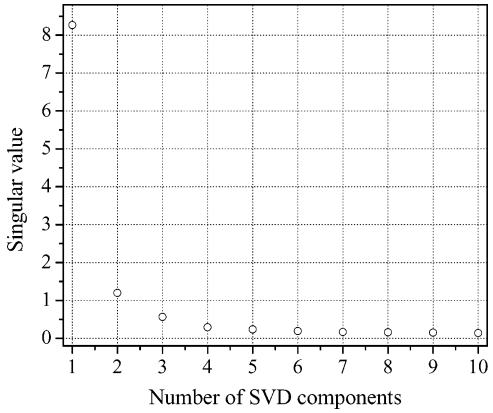


**Figure 2.** Singular values obtained from the SVD analysis of time-resolved difference absorbance spectra of ATRA in hexanol.

Both all-*trans*-retinal and the ATRA molecules have approximately a $C_{2h}$ symmetry, which is the same as those polyene molecules. The symmetrical different single excited states of polyene molecules including carotenoids have been extensively studied both theoretically and experimentally.[33−35] The ordering of the excited singlet states of polyenes, that is, $1B_u^+$, $1B_u^-$, and $2A_g^-$, has also been studied theoretically[36] and experimentally,[37,38] and it is expected that in carotenoids, for $n \leq 8$ ($n$ is the number of the conjugated double bonds), the lowest optical-transition-allowed singlet state should be $1B_u^+$,[39] and an optically forbidden state, $2A_g^-$, is closely located under the $1B_u^+$ excited manifold. As for all-*trans*-retinal, in addition to this $2A_g^-$ state, there also exists another low-lying optically forbidden state, $n\pi^*$, in polyene aldehydes. It is known that there are three excited singlet states existing in the lowest-energy region up to 30 000 $cm^{-1}$,[35,40,41] and the ordering of these excited singlet states has been determined recently by ultrafast spectroscopic studies. A recent femtosecond time-resolved transient absorption study and also a femtosecond time-resolved fluorescence up-conversion study of all-*trans*-retinal show that $S_3$ is of $B_u^+$ character, $S_2$ is of $n\pi^*$ character, and $S_1$ is of $2A_g^-$ character.[32,42] In contrast, the excited singlet states and their relative energy ordering of ATRA are still unclear. Sahyun et al investigated the excited states of ATRA, as well as that of ATRA−$TiO_2$. They found evidence supporting two closely spaced singlet excited states assigned as $n\pi^*$ ($S_1$) and $\pi\pi^*$ ($S_2$). Their picosecond time-resolved transient absorption results showed that a transient absorption peak at 450 nm with a lifetime of 35 ps in ATRA−methanol solution was observed and was assigned to the $S_1$ absorption,[43] while Bondarev et al reported this value to be 80 ps in 90:10 hexane/ether solvent.[44]

Referring to the three principal singular values obtained in the SVD analysis and with analogue to the excited singlet-state photophysics of retinal, we propose the kinetic scheme in Scheme 2 for the photophysics of ATRA. In this proposed kinetic scheme, $S_3$ is populated by direct Franck−Condon

**SCHEME 2: Relaxation Kinetics for the Excited Singlet Manifolds of ATRA**

$$S_3 \xrightarrow{k_3} S_2 \xrightarrow{k_2} S_1 \xrightarrow{k_1} S_0$$

**TABLE 1: Rate Constant for ATRA in Hexanol**

| singlet state (peak position, nm) | rate constant ($ps^{-1}$) | time constant (ps) |
|---|---|---|
| $S_3$ (580) | 9.8 ($k_3$) | 0.10 |
| $S_2$ (470, 553) | 0.46 ($k_2$) | 2.2 |
| $S_1$ (460, 553) | 0.074 ($k_1$) | 25.5, 41.5[a] |

[a] Direct fitting from the experimental kinetic curve at 450 nm.

transition, while the optical transitions from $S_0$ to $S_1$ and $S_2$ are not allowed. These two states can only be populated through internal conversion (IC) and finally relax to the ground state. Accordingly, the population change of the individual species is described by the following set of equations:

$$[S_3] = \exp(-k_3 t)$$

$$[S_2] = \frac{k_3}{k_2 - k_3}[\exp(-k_3 t) - \exp(-k_2 t)]$$

$$[S_1] = k_3 k_2 \left[\frac{\exp(-k_3 t)}{(k_2 - k_3)(k_1 - k_3)} + \frac{\exp(-k_2 t)}{(k_3 - k_2)(k_1 - k_2)} + \frac{\exp(-k_1 t)}{(k_3 - k_1)(k_2 - k_1)}\right]$$

By global fitting the spectra and kinetics of the singlet excited manifolds $S_3$, $S_2$ and $S_1$, we obtain the corresponding spectra and population curves of the individual components as shown in Figure 3. The fitted curves were convoluted to match the experimental data by using a Gaussian type of instrumental response function with a fwhm of 0.22 ps. The fitted lifetime constants of the excited states are listed in Table 1. The rising phase of $S_3$ shows that it is beyond the instrumental resolution (150 fs), while $S_2$ and $S_1$ have a rising time of 0.1 and 2.2 ps, respectively. These results are consistent with the proposed scheme that the two lower excited singlet states are populated from $S_3$ via IC.

**Femtosecond Time-Resolved Absorbance Difference Spectra of ATRA−$TiO_2$.** Figure 4 shows seven chirp-corrected time-resolved absorbance difference spectra of ATRA−$TiO_2$ in hexanol solution purged with Ar gas excited at 400 nm. Compared to that of free ATRA, two salient features should be noticed. The first is the transient absorbance at 620 nm with a rather slower decay kinetics. The second is that the gradually formed 450 nm absorption within about 100 ps almost does not decay up to 900 ps limited by the traveling range of the translation stage. Furthermore, the fast decay component of 620 nm absorption (19.8 ps) well correlates to the rising of 450 nm absorption (19.0 ps) as shown in Figure 5. A detailed analysis will be given in the later section. Figure 6 presents both the normalized submicrosecond time-resolved triplet absorption spectrum of ATRA−$TiO_2$ in hexanol delayed at 10 $\mu$s excited at 355 nm and femtosecond time-resolved difference absorption spectrum delayed at 250 ps excited at 400 nm. The almost superimposition of these two spectra within the observable region indicates that the observed long-lived component peaked at 450 nm is derived from the ATRA triplet-state absorption. The 620 nm absorption peak found in the femtosecond time-resolved spectra also have a slow decaying phase, which can still be observed in the microsecond temporal region. This is

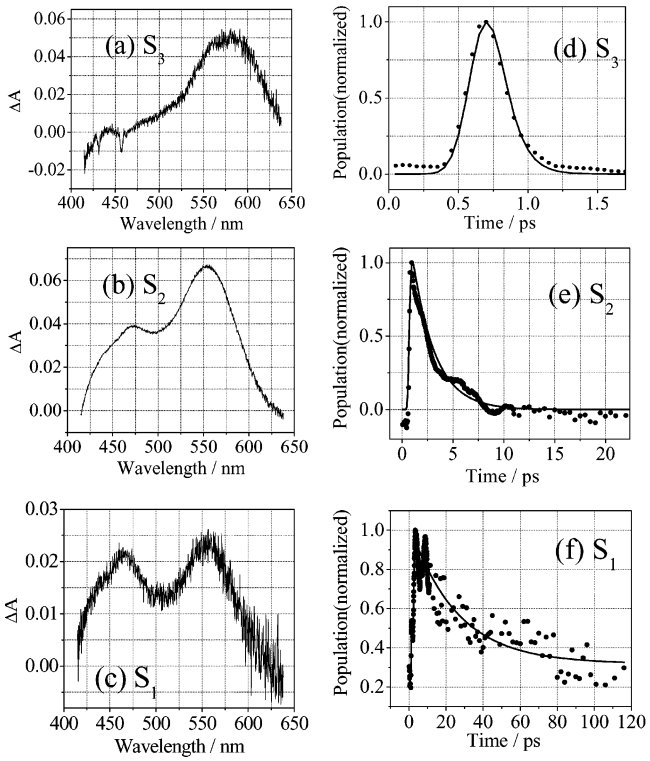


**Figure 3.** Spectra (a−c) and populations (d−f) of the three transient species resolved by SVD analysis and global fitting from time-resolved difference absorbance spectra of ATRA in hexanol.

**SCHEME 3: Excited-state Relaxation, Electron Injection and Charge Recombination Kinetics for ATRA−$TiO_2$ Nanoparticle**

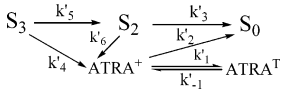


attributed to the absorption of the ATRA radical cation on the $TiO_2$ surface.[24] SVD analysis and global fitting are employed to resolve the spectra and the population kinetics of the components. The results of the SVD analysis of ATRA−$TiO_2$ is displayed in Figure 7, which shows that the time-resolved absorption spectra of ATRA−$TiO_2$ in hexanol has the following principal singular values: 6.3121, 1.3069, 0.8215, 0.2895, 0.2202, 0.2024, 0.1793, 0.1633, 0.1433, and 0.1328. The fifth- and higher-order singular values are smaller than 0.2024, and their contributions are regarded as noise.

In this experiment, the excitation power is 5 $\mu$J/pulse with a focal beam size of about 500 $\mu$m. The flowing sample cell has an optical path length of 2 mm. The $TiO_2$ nanoparticles have an average size of 1.4 nm. The optical density measured for ATRA−$TiO_2$ in hexanol at 400 nm is 0.05 (2 mm path length). The calculated concentration for the absorbed photon and the average concentration of $TiO_2$ particles are $2.5 \times 10^{-5}$ and $5.6 \times 10^{-4}$ M ($d = 1.4$ nm for $TiO_2$ nanoparticle is taken for the calculation), respectively. According to this simple estimation, it can be inferred that about one ATRA molecule is excited for every ATRA adsorbed $TiO_2$ nanoparticle; therefore, the bimolecular recombination process can be excluded. Compared to the photophysics of the free ATRA, electron transfer to the $TiO_2$ conduction band and the subsequent charge recombination to the triplet and ground states are included for ATRA−$TiO_2$ as shown in Scheme 3.

It is possible that the lower excited singlet states $S_2$ and $S_1$ may also undergo interfacial electron transfer, while the $S_1$ state

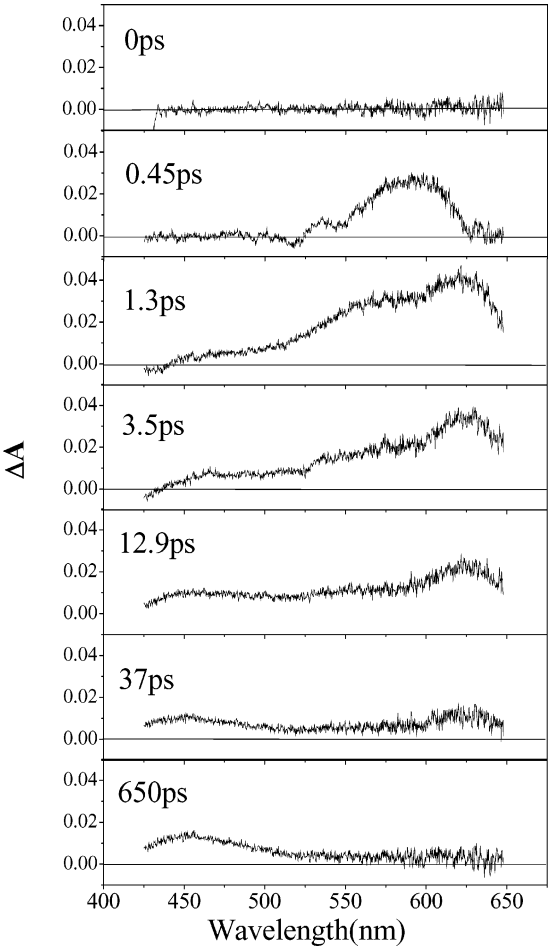


**Figure 4.** Seven chirp-corrected time-resolved absorbance difference spectra of ATRA−$TiO_2$ in hexanol purged with Ar gas excited at 400 nm, 5 $\mu$J/pulse.

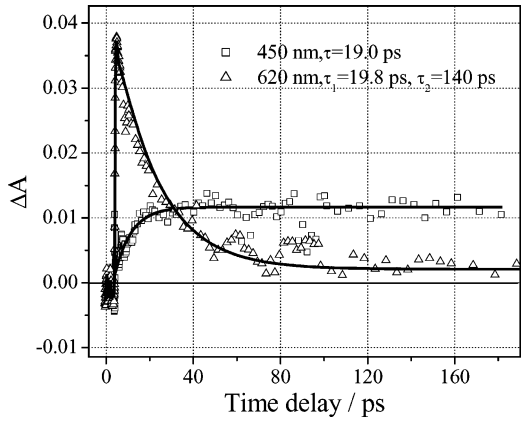


**Figure 5.** Kinetics probed at (△) 620 and (□) 450 nm by 400 nm photoexcitation of ATRA−$TiO_2$ in hexanol. Solid lines represent fitted curves.

($2A_g^-$) is covalent in character with a lower electron-injection efficiency.[25] Therefore, in the present case, electron injection from $S_1$ is not included; only four intermediate species, $S_3$, $S_2$, $ATRA^+$, and $ATRA^T$, are proposed in the global fitting analysis. In fact, we have tried to incorporate the $S_1$ state in the global fitting analysis; however, resolution of the $S_1$ absorption spectrum and the corresponding population kinetics were not successful. In our earlier experiment, we found that in the microsecond time domain $ATRA^+$ and $ATRA^T$ have almost a same decay time constant of 40.0 and 39.2 $\mu$s, respectively, which reveals a possible electron injection channel from $ATRA^T$ to the conduction band of the $TiO_2$ nanoparticle. This finally can lead to an equilibrium between $ATRA^T$ and $ATRA^+$. In the global fitting, only the early-time kinetics is considered, where the electron injection from $ATRA^T$ to the conduction band of $TiO_2$ is neglected. The obtained rate constants for the four intermediate species are listed in Table 2. Figure 8 shows the global fitting results of the individual spectra and the corresponding population curves of the four components.

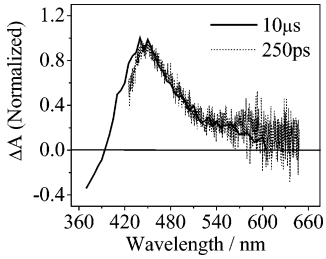


**Figure 6.** Microsecond time-resolved triplet absorption spectrum of ATRA−$TiO_2$ in hexanol delayed at 10 $\mu$s in hexanol excited at 355 nm and femtosecond time-resolved difference absorption spectrum delayed at 250 ps excited at 400 nm.

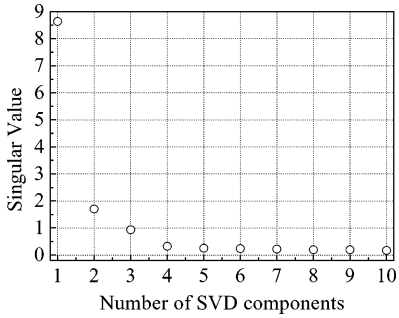


**Figure 7.** Singular values obtained from the SVD analysis of time-resolved difference absorbance spectra of ATRA−$TiO_2$ in hexanol.

**TABLE 2: Rate Constant and Time Constant for ATRA−$TiO_2$ with Model 1**

| species (peak position, nm) | rate constant ($ps^{-1}$) | rise (ps) | decay (ps) |
|---|---|---|---|
| S3 (591) | 2.8 ($k'_4 + k'_5$) | | 0.36 |
| S2 (558, 623) | 0.98 ($k'_3 + k'_6$) | | 1.0 |
| cation | 0.047 ($k'_1 + k'_2$) | | 21.1 |
| (575 shoulder, 626) | | | $9.8 \pm 2.1$,[a] 140[a] |
| triplet (450) | | $19.0 \pm 0.8$[b] | |

[a] Biexponential decay time constants obtained by fitting of the experimental kinetic curve at 620 nm. [b] Time constants obtained by fitting of the experimental kinetic curve at 450 nm.

## Discussion

**1. Excited Singlet States of Free ATRA.** Though the excited singlet manifolds of ATRA in methanol have been studied by picosecond time-resolved difference absorbance spectra,[43] further investigation of better temporal resolution is necessary to make a clearer assignment. Some analogues can be made in line with that of all-*trans*-retinal the excited-state absorption spectra of which have been assigned.[45,30,32] Our SVD analysis of femtosecond time-resolved absorption spectra of ATRA unambiguously shows that there are at least three excited transient species, and the global fittings successfully resolved each of the components. Because the triplet absorption has not been observed by either femtosecond time-resolved spectroscopic measurement or submicrosecond flash photolysis, we conclude that the quantum efficiency for the intersystem crossing from the excited singlet to the triplet is low. This is qualitatively

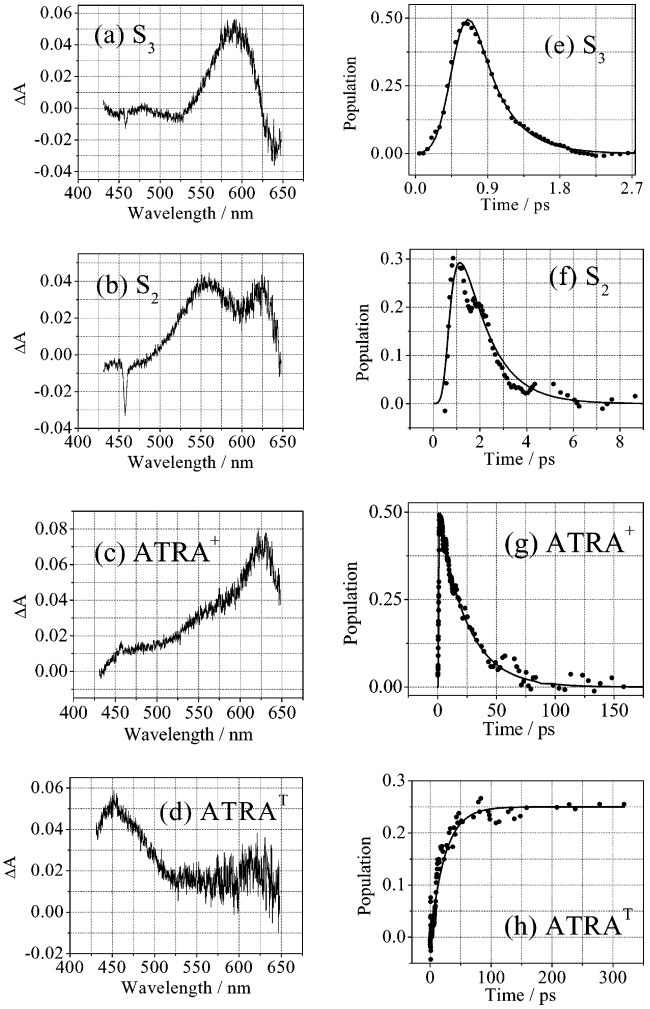


**Figure 8.** 8 Spectra (a−d) and populations (e−h) of four intermediate species resolved by SVD analysis and global fitting from time-resolved difference absorbance spectra of ATRA−$TiO_2$ in hexanol.

in agreement with the reported intersystem crossing efficiency with a value of 0.012 for ATRA.[46] Therefore the three excited states can be assigned as the excited singlet states $S_3$, $S_2$, and $S_1$.

In the recent femtosecond time-resolved difference-absorption spectroscopic studies of all-*trans*-retinal, three excited singlet states have been observed. All of the absorption spectra of $S_3$, $S_2$, and $S_1$ have a broad absorption in the visible region from 400 to 800 nm with well-defined peak positions at different wavelengths. The $S_3$ state has an absorption peak around 605 nm, the $S_2$ state has two peaks around 480 and 540 nm, and $S_1$ state has a peak around 450 nm. The rise time for $S_3$ and $S_2$ are too short to be determined, and femtosecond time-resolved absorption spectra (150 fs resolution) of all-*trans*-retinal cannot distinguish whether the $S_2$ state is populated by direct photoexcitation or by IC from the $S_3$ state.[30] Yet Tahara et al studied the fluorescence of all-*trans*-retinal with a time-resolved upconversion technique, they concluded that $S_3$ is of $B_u^+(\pi,\pi^*)$ character and the $S_3 \leftarrow S_0$ transition contributes to about 96% of the ground-state absorption;[32] thus it is plausible to assume that the $S_2$ and $S_1$ states are populated by the IC process. Judged on the close resemblance in the molecular structures of all-*trans*-retinal and ATRA, it is expected that the excited-state photophysics of ATRA should be similar to that of all-*trans*-retinal. However the additional hydroxyl group of the carboxylic group might cause a shift in the energy level of the n$\pi^*$ state with respect to that of all-*trans*-retinal.

As shown in Figure 3a, the time-resolved transient absorption spectra of ATRA for the $S_3$ state has a broad absorption with a peak at 580 nm, the $S_2$ state has a double-peaked structure with a major absorption at 553 nm and a minor absorption at 470 nm, and the $S_1$ state also has a double-peaked absorption with two absorption maxima of almost equal intensity at 460 and 553 nm. The lifetimes for $S_3$, $S_2$, and $S_1$ by global fittings are 0.1, 2.2, and 25.5 ps (direct fitting of the experimental curve at 450 nm by biexponential decay results in a slow decay component of 41.5 ps), respectively. Compared to the excited-singlet state absorption spectra of all-*trans*-retinal, the photophysical properties of $S_3$ are quite similar. The fast rising beyond the limit of detection suggests that it is an optically allowed singlet state, and it undergoes a very efficient IC with a time constant of 0.1 ps. Thus we assign $S_3$ as the $1B_u^+$ state of the retinyl moiety. A remarkable difference between all-*trans*-retinal and ATRA lies in that the former has an appreciable magnitude in the intersystem crossing quantum yield while that for the latter almost cannot be detected. The quantum yield for the triplet formation of all-*trans*-retinal in hexane is reported to be as high as 0.74,[30] and the intersystem crossing from $S_1$ to $T_1$ is of a unit efficiency. The large intersystem crossing efficiency for all-*trans*-retinal can be interpreted by the electronic configuration of $S_1$ state. Taking the lowest excited triplet state $T_1$ to be of $\pi$ character ($\pi\pi^*$,$1^3B_u^+$),[47] in all-*trans*-retinal the $S_1$ state is of n$\pi^*$ character, and the intersystem crossing occurs between $S_1$ (n$\pi^*$) and $T_1$ ($\pi\pi^*$,$1^3B_u^+$) states. According to the El-Sayed rule for the relationship between the ISC efficiency and the electronic configuration of the excited states, which states that the ISC between the excited states with different electronic configurations ($^1$n$\pi^* \leftrightarrow {}^3\pi\pi^*$, $^1\pi\pi^* \leftrightarrow {}^3$n$\pi^*$) takes place efficiently, while that between the same configuration ($^1$n$\pi^* \leftrightarrow {}^3$n$\pi^*$, $^1\pi\pi^* \leftrightarrow {}^3\pi\pi^*$) is, in principle, prohibited.[48,49] As to the $S_1$ state of ATRA, both $2A_g^-$ ($^1\pi\pi^*$) and n$\pi^*$ can be the candidates. However, if n$\pi^*$ is assigned as the $S_1$ state, it is expected that the ISC should be very efficient, which would give rise to an appreciable quantum yield of triplet state. Because this has not been observed in the experiments, in fact, the quantum yield for the triplet state of ATRA is smaller than that of all-*trans*-retinal by an order of 2 in magnitude, we assign the lowest excited-state $S_1$ of $2A_g^{-1}$ ($\pi\pi^*$) character, which arises from the retinyl chromorphore.

Compared with that of all-*trans*-retinal, the n$\pi^*$ absorption spectra are similar in both the spectral region and peak absorption wavelengths; however, their relative intensities vary. In ATRA, the major absorption peak is located in the red side at 553 nm and a minor absorption at 470 nm in the blue side, while in all-*trans*-retinal, the relative peak absorption intensity is reversed. This can be accounted by the effect of hydroxyl group, because it can directly affect the energy level of the lone pair electrons. An energy level diagram for the excited singlet manifolds is summarized in Figure 9. A remarkable difference for the excited singlet manifolds between ATRA and all-*trans*-retinal is that the energy level ordering for $2A_g^-$ and n$\pi^*$ is reversed.

An apparent difference for the observed $S_1$ absorption spectra between our experiment and the result of Sahyun et al. should be noticed. In their experiment, a single absorption peak at 450 nm with a lifetime of 35 ps is assigned as the $S_1$ absorption.[43] In our experiment, a double-peaked absorption (460 and 553 nm) is observed for $S_1$ absorption, and this absorption spectrum does not rely on the SVD analysis because the lifetime of $S_3$ and $S_2$ are very short compared to that of $S_1$ and this double-peaked absorption remains after the complete decay of $S_3$ and

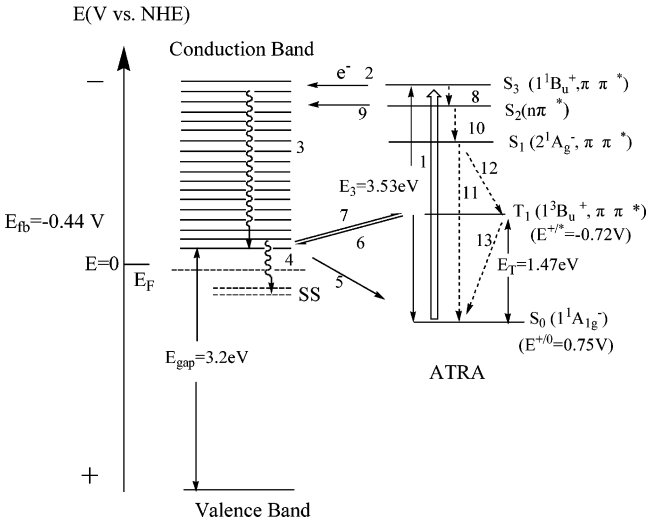


**Figure 9.** Schematic diagram of energy levels for ATRA and photoinduced interfacial electron injection and charge recombination processes in ATRA−$TiO_2$ nanoparticle in hexanol: (1) photoexcitation; (2, 6, 9) electron injection from $S_3$, $T_1$, and $S_2$; (3) energy relaxation of the injected electron to the bottom of the conduction band; (4) electron trapped at surface state (SS); (5) charge recombination to the ground state; (7) charge recombination to the triplet; (8, 10, 11) internal conversion; (12) intersystem crossing; (13) nonradiative decay from $T_1$ to the ground state. $E_F$ = Fermi level; $E_{fb}$ = flat band potential calculated at pH = 3.0 against NHE;[63] $E^{+/0}$ = reduction potential for $ATRA^+$/ATRA in 90:10 acetonitrile−methanol;[43] $E^{*/0}$ = reduction potential for $ATRA^{+/3}$ATRA; $E_3$ = the lowest optically allowed transition energy; $E_T$ = the energy difference between the lowest triplet state and the ground state based on the ester-like linkage form of ATRA on $TiO_2$ nanoparticle in hexanol.[50]

$S_2$ states. The discrepancy can arise from the photoionization effect in the experiment of Sahyun et al., where the photoionized product $ATRA^+$ has an absorption at 580 nm, which could interfere with the observation of the red-side absorption peak of $S_1$ at 553 nm. According to our femtosecond time-resolved spectroscopic study, their assignment of $S_1$ as the n$\pi$* state based on the result of picosecond laser photolysis is probably inappropriate.

**2. Electron Injection from the Excited Singlet States of ATRA to $TiO_2$.** The energy levels for the ATRA excited singlet states and those of the conduction and valence band for $TiO_2$ are shown schematically in Figure 9. All of the energy levels of the excited singlet manifolds are above the bottom of the conduction band, which may give rise to all the three excited singlet states having the possibility to inject one electron into the conduction band of $TiO_2$ nanoparticles. It has been shown that ATRA is chemically bound to the $TiO_2$ surface through formation of an ester-like linkage, bridge, and chelating between the carboxylic group and the titanium surface atom,[50] and ultrafast spectroscopic study reveals that the injection of electron from the excited state of the dye adsorbates to the $TiO_2$ conduction band in a chemically bound form via the carboxylic group can be as fast as <50 fs.[51−53] Therefore, in the present case, a fast electron injection process should be expected. As shown in Figure 8, $S_3$ has an absorption peak at 591 nm. Compared to that of the free ATRA, the absorption peak is slightly red-shifted by 11 nm, whereas its kinetics also has a fast rising beyond the resolution of the instrument. However its decay rate of 1/0.35 $ps^{-1}$ is smaller than that of the free ATRA (1/0.1 $ps^{-1}$). Obviously this decay rate of $S_3$ for ATRA−$TiO_2$ is a sum of the two parts; one is the electron injection rate ($k_4'$) and another is the IC rate ($k_5'$), that is, 1/0.35 ($ps^{-1}$) = $k_4' + k_5'$; thus, we can assign an upper limit for both the electron injection and IC rates, that is, $k_4' < 1/0.35$ ($ps^{-1}$) and $k_5' < 1/0.35$ ($ps^{-1}$). The interfacial electron injection rate is apparently smaller than those of direct electron injection systems which involve injection of an electron from the dye to the $TiO_2$ conduction band directly by photoexcitation with a typical rate larger than 1/50 ($fs^{-1}$).[54,55] The present system apparently falls into those of indirect electron injection, where an excited state of the dye molecule is initially formed and then transfers an electron to the particle from the excited states.[56,57] It is worth noting that the upper limit for the electron injection rate is consistent with that of a closely resembled system, that is, all *trans*-8′-apo-$\beta$-caroten-8′-oic acid/$TiO_2$, where an electron injection rate of 1/0.36 ($ps^{-1}$) has been observed.[25] Compared to the free ATRA in hexanol, the IC rate of ATRA−$TiO_2$ becomes smaller. This possibly arises from the fact that when ATRA is adsorbed onto $TiO_2$, the freedom of motion either for the molecule as a whole or for the internal atoms is reduced. Because the IC needs the coupling of the vibrational modes to the two electronic states,[58] the partial "freezing" of the vibrational modes would lead to a less-efficient IC, which could account for the observed smaller IC rate for ATRA−$TiO_2$. For the $S_2$ state, it decays faster in ATRA−$TiO_2$ ($k_3' + k_6' = 1/1.0$ ($ps^{-1}$)) than that in the free ATRA (1/2.2 ($ps^{-1}$)). Assuming the IC rate for ATRA−$TiO_2$ is the same as that of ATRA, that is, $k_3' = 1/2.2$ ($ps^{-1}$), then the electron injection rate for $S_2$($k_6'$) can be derived with a value of 1/1.8 ($ps^{-1}$). Therefore it can be concluded that the $S_2$ (n$\pi$*) state of ATRA also has a fairly strong electron injection capability. Though resolution of the $S_1$ component was not successful, we have inspected the kinetics probed at 450 nm, which would comprise mainly that from the $S_1$ state and the triplet state; in the early time, we can only observe a constant rising phase, which indicates that the contribution of $S_1$ state would be negligible. This is plausible because the interfacial electron injection process competes with IC in both $S_3$ and $S_2$ state, which would substantially reduce the quantum yield for the formation of the $S_1$ state. This also justifies the neglect of the $S_1$ state in Scheme 3 for the global fitting. Comparing the absorption spectra of $S_2$ (n$\pi$*) of free ATRA and that of the adsorbate on the $TiO_2$ nanoparticle, the absorption peak at 553 nm of free ATRA is slightly red-shifted to 558 nm in ATRA−$TiO_2$, while the blue-side absorption peak at 470 nm disappears; instead, a new absorption peak at 623 nm can be observed. This peak may arise from the n$\pi$* absorption owing to the formation of an ester-like or a chelating linkage between the carboxylic group and the titanium surface atoms.

**3. Charge Recombination between the Trapped Electron and the ATRA Radical Cation.** Charge recombination to the triplet states in the optically excited systems is less frequently observed than that to the ground state. It is because that initially charge-separated germinate radical ion pair bears the same spin state as the singlet excited-state precursor. When a singlet radical ion pair recombines to the excited triplet state, a spin flipping must be involved. As observed in the photoexcitation of the D−A system, the photoinduced charge separation leads to the formation of the singlet radical ion pair $^1[D^+-A^-]$, while the spin mixing induced by Zeeman and hyperfine interaction allows the intersystem crossing within the radical ion pair $^1[D^+-A^-]$ forming a spin-correlated triplet radical ion pair $^3[D^+-A^-]$. The subsequent charge recombination within the triplet radical ion pair $^3[D^+-A^-]$ leads to the formation of the triplet species.[59] Therefore for intramolecular charge recombination, only the germinate pair recombination is encountered. However when charge recombination does not occur within a germinate pair,

that is, the spins of the electron and the radical ion are totally uncorrelated, the charge recombination follows the statistics of the spin multiplicity, which leads to 25% singlet and 75% triplet species. Such a recombination is termed as homogeneous recombination. For intermolecular charge recombination in a very polar solvent, the radical ion can diffuse out of the solvent cage, and spin correlation no longer holds, leading to a homogeneous recombination. Thus spin flipping is not necessary in a homogeneous recombination. This has been observed in a system of pyrene plus 3,5-dimethoxy-dimethylaniline in methanol by Schulten et al.[21]

For interfacial electron transfer, electrons are initially injected into the particle above the conduction band, and relax very fast to the bottom of the conduction band. Then the injected electrons are trapped with different trapping depth and migrate from one trap to another on the surface of the $TiO_2$ nanoparticles. The above electron relaxation and trapping process has been observed in a time scale of 100 fs.[60,61] When the trapped electron undergoes charge recombination with the oxidized dye radical cation, it follows a homogeneous recombination rather than a germinate recombination. Therefore solely on the basis of the spin statistics, the interfacial back electron transfer, in principle, provides a very promising system for the observation of charge recombination to the triplet state. Yet it has rarely been observed because the driving force also plays a crucial role in governing the electron-transfer path. It has been shown in many cases that the interfacial electron-transfer rate also follows the Marcus equation. For weak coupling at the nonadiabatic limit, the rate equation can be written as

$$k_{CR}(r) = \sqrt{\frac{\pi}{\hbar^2 \lambda(r) k_B T}} V(r)^2 \, e^{-[\Delta G_{CR} + \lambda(r)]^2/(4\lambda k_B T)} \qquad (1)$$

where $r$, $\lambda(r)$, $V(r)$, and $-\Delta G_{CR}$ are the distance between the trapped electron and cation, reorganization energy, electronic coupling matrix element, and the driving force, respectively.[62−64] For those adsorbed molecules such as ATRA the triplet energy level of which is higher above the bottom of the conduction band, the charge recombination to the triplet state is an endothermic process, while to the ground state it is an exothermic process; for most cases, this will lead to the charge recombination to the ground-state overwhelming that to the triplet state. However, this situation can be reversed when the triplet energy level is close to that of the trapped electron and meanwhile the charge recombination to the ground state is within the Marcus inverted region. Because the predominance of charge recombination to the triplet state should satisfy the above prerequisites simultaneously, it may account for the rare observation of charge recombination to the triplet state even in an interfacial electron-transfer process.

Interfacial charge recombination kinetics is rather complicated because of the random distribution of the trapped electron on the $TiO_2$ surface with a varied charge separation distance, $r$, which gives rise to a highly non-single-exponential feature of the recombination kinetics.[55] A lifetime of 40 $\mu$s has been observed for the charge recombination in ATRA−$TiO_2$ in the microsecond time domain, which also reflects such an interfacial character.[24] In the early time, the charge recombination kinetics correspond to those of cation and the trapped electron at the closest contact. Therefore, the charge separation distance on the early time kinetics is considered as fixed at the closest contact. As shown in the Scheme 3, the charge recombination proceeds via two channels to the triplet and ground state, respectively. As the population of the triplet state builds, the excited triplet state can reinject an electron back into the $TiO_2$ nanoparticle. Thus a steady state for $ATRA^T$ can be expected, which is confirmed in Figure 5 in which a plateau appears in the kinetics of $ATRA^T$ (probed at 450 nm) beginning at about 20 ps. Therefore in the early time, the $ARTA^+$ recombination rate, $k_{rec}$, is a sum of the rates for $ATRA^+$ recombining both to the triplet ($k_1'$) and to the ground state ($k_2'$). After the steady state of $ATRA^T$ is reached, the relation $k_{rec} = k_2'$ should be realized. Therefore the decay kinetics of $ARTA^+$ can be approximately regarded as a biexponential process with decay time constants of $1/(k_1' + k_2')$ and $1/k_2'$. Fitting of the kinetics for $ATRA^+$ probed at 620 nm with a biexponential decay results in two decay time constants of 19.8 and 140 ps and a ratio for the preexponential factor of 6.0 (population branch ratio for charge recombination to the triplet and ground state). Thus $k_2 = 1/140$ ($ps^{-1}$) and $k_1 = 1/17.4$ ($ps^{-1}$). Meanwhile direct fitting of the $ATRA^T$ kinetics gives a monoexponential rising time constant of 19.0 ps, giving $k_1$ a value of 1/19.0 ($ps^{-1}$). As to the global fitting analysis, the electron injection from the triplet state to the $TiO_2$ nanoparticle is not considered; therefore, only $1/(k_1' + k_2')$ is obtained, which has a value of 1/21.1 ($ps^{-1}$), leading to $k_1' = 1/18.3$ ($ps^{-1}$). Obviously the rate constant $k_1$ evaluated by three different ways has a consistent value, that is, fitting of the $ATRA^+$ decay kinetics, $ATRA^T$ rising phase, and global fitting give a value of 1/17.3, 1/19.0, and 1/18.3 ($ps^{-1}$), respectively. Selecting 1/19.0 ($ps^{-1}$) for $k_1'$ shows that the charge recombination to the triplet state is 7.4 times faster than that to the ground state (kinetic branch ratio). The discrepancy between the population and kinetic branch ratios could arise from the fact that when calculating the kinetic branch ratio the electron injection from the ATRA triplet state is not included, leading to a larger value for the kinetic branch ratio. After correction for the spin statistics, this ratio becomes 2.5. Yet the spin-statistics-corrected rate of charge recombination to the triplet state (1/57.0 ($ps^{-1}$)) is still faster than that for IP-ISC mechanism ever observed even in the covalently linked donor−acceptor pair where the coupling is strong.[19,20] Therefore the observed fast charge recombination rate favors the triplet state being generated by the direct charge recombination rather than by the IP-ISC mechanism.

If we assume that the difference between the charge recombination to the ground state and that to the triplet state is only caused by the difference in the driving force, then the reorganization energy can be calculated according to eq 1, that is, $k_{CR}^S/k_{CR}^T = \exp\{-[(\Delta G_{CR}^S + \Delta G_{CR}^T + 2\lambda)(\Delta G_{CR}^S - \Delta G_{CR}^T)]/(4\lambda k_B T)\}$, where superscripts S and T stand for the charge recombination to the ground and the triplet states, respectively, $\Delta G_{CR}^G = -1.2$ eV, and $\Delta G_{CR}^T = 0.3$ eV.[24,50] The ratio between the rate for charge recombination to the ground state and that to the triplet state has a value of 1/2.5. This results in a value of reorganization energy of 0.44 eV. The derived reorganization energy for the interfacial charge recombination is in agreement with what has been observed for a series of dye chemically bound to $TiO_2$ nanoparticles in magnitude, where the reorganization energy lies in a region between 0.3 and 0.6 eV.[63] With the calculated reorganization energy, we further calculated the electronic coupling matrix element $V(r)$ of charge recombination to both the triplet and ground state according to eq 1, which gives rise to an apparent electronic coupling matrix element $V(r)^T$ of 5188 $cm^{-1}$ (0.64 eV) for charge recombination to the triplet state and 2670 $cm^{-1}$ to the ground state (0.33 eV). Thus it is concluded that both charge recombination to the triplet state and that to the ground state are strongly coupled, beyond the nonadiabatic limit (0.1 eV).[65] These results also show that in

fact the electronic coupling matrix elements for charge recombination to the triplet state and the ground state are not equal; the ratio between these two electronic coupling matrix elements deviates from the presumed unity by a factor of 1.95, showing the deviation imposed by the nonadiabatic limit when it is applied to a strong coupling adiabatic system. The observed large apparent electronic coupling matrix elements in magnitude for interfacial charge recombination seemingly contradict to the reported values, where $V(r)$ of several $cm^{-1}$ has been reported for a number of dyes chemically bound to $TiO_2$ nanoparticle surface[63] and of 30 $cm^{-1}$ for some inorganic dyes electrostatically bound to ZnO nanoparticle.[64] Because it has been suggested that the highly non-single-exponential character of interfacial charge recombination mainly arises from the charge recombination of a distributed electron−cation separation distance, it is noted that the reported electronic coupling matrix elements are evaluated from the charge recombination kinetics at a time domain of microseconds, which clearly corresponds to kinetics of charge recombination at a larger separation distance. $V(r)$ has a monoexponential decay dependence on $r$, that is, $V(r)^2 = V_0^2\, e^{-\beta r}$, where $V_0$ is the electronic coupling matrix element at the closest contact and for most of the organic medium $\beta$ is around 1/1.4 $Å^{-1}$.[66,67] If we also use a rate constant of 1/40 $\mu s^{-1}$ observed in the charge recombination for ATRA−$TiO_2$ in the microsecond domain, an electronic coupling matrix element for charge recombination to the triplet state is obtained with a value of 3.6 $cm^{-1}$, which is consistent with the reported values for dye/$TiO_2$. Therefore the observed electronic coupling matrix element for the microsecond domain reflects its decay over a distance because of the delocalization of the trapped electron. If we employ $V_0^T = 5188$ $cm^{-1}$ for the electronic coupling matrix element of charge recombination to the triplet state at the closest contact, where the trapped electrons are localized at the titanium atoms bound to ATRA, and $V(r)^G = 3.6$ $cm^{-1}$ for the furthest delocalized trapped electrons, then a delocalization radius can be evaluated as $r = 2.0$ nm for charge recombination through the organic medium as shown in Scheme 1. It is noteworthy that this result is consistent with the previous study of particle-size-independent non-single-exponential dynamics of charge recombination for $Fe(II)(CN)_6^{4-}/TiO_2$ nanoparticle, in which the highly non-single-exponential decay kinetics from picoseconds up to 1 ns was fitted with a trapped electron distribution model leading to a possible maximum distance of the injected electron away from the adsorbate of about 2.3−3.6 nm when the lower limit of the electron effective mass is considered.[55]

Our observation is also relevant to the EL device. For the fluorescence type of EL device, charge recombination to the triplet state leads to an inefficient electron−photon conversion due to the optical-transition forbidden character of the triplet state. In EL process, the electron and hole is generated independently, which breaks the spin correlation, and a homogeneous recombination is expected. Such a recombination would lead to 25% of fluorescence solely based on the consideration of the spin statistics. However, if the exciton state is weakly coupled, the charge recombination is not only governed by the spin statistics but also determined by the driving force, where eq 1 might also be valid. Because the charge recombination to the excited singlet state leading to fluorescence always has a smaller driving force than that to the triplet state, if the reorganization energy is larger than the driving force for the triplet state, charge recombination to the triplet state is more favorable than that to the excited singlet state, which leads to the fluorescence efficiency less than 25%. However, if the reorganization energy is smaller than the driving force to the triplet state, the charge recombination to the triplet state would be in the Marcus inverted region, whereas charge recombination to the excited singlet state would be faster, which gives a good chance to achieve a fluorescence efficiency better than the limit imposed by the spin statistics. In recent research, EL fluorescence efficiency better than 50% has been reported,[8] which clearly breaks the limit imposed by the spin statistics. Though parameters such as the reorganization energy and the electronic coupling matrix element in EL systems are not clear yet, the present work provides a possible mechanism by which the EL device may exceed the limit of the spin statistics.

## Conclusions

The excited-state dynamics of the free ATRA in hexanol, the electron injection of ATRA bound to $TiO_2$ nanoparticle, and the subsequent charge recombination have been studied by using femtosecond time-resolved visible difference absorption spectroscopy. Three excited singlet manifolds, that is, $S_3$, $S_2$, and $S_1$ have been observed for the ATRA molecule after 400 nm photoexcitation. $S_3$ is assigned as an optically allowed singlet state $1B_u^+$, while $S_2$ and $S_1$ are assigned as $n\pi^*$ and $2A_g^-$ ($\pi\pi^*$), respectively. Different from the early picosecond time-resolved spectroscopic study, the lowest excited singlet state is assigned as $2A_g^-$ ($\pi\pi^*$) instead of $n\pi^*$. The energy ordering for these lowest two excited singlet states is reversed compared to that of all-*trans*-retinal.

When ATRA is chemically bound to a $TiO_2$ surface, it is found that at least two higher excited singlet states can inject electron into the $TiO_2$ conduction band with an electron injection rate of $<1/0.35$ ($S_3$) and 1/1.8 ($ps^{-1}$) ($S_2$). The charge recombination between $ATRA^+$ and the trapped electron is expected to be a homogeneous recombination following the spin statistics. The branching ratio for the population on the excited triplet state and the ground state during the charge recombination is observed as 6.0, while the ratio between the charge recombination rate to the triplet state and that to the ground state is 7.4. After the correction of the spin statistics, this ratio becomes 2.5. On the basis of the assumption that the difference in the rates for charge recombination to the triplet state and ground state is caused only by the driving force difference, the reorganization energy can be calculated as 0.44 eV under the nonadiabatic limit, a typical value of reorganization energy for interfacial charge recombination of dye chemically bound to $TiO_2$ surfaces. The apparent electronic coupling matrix elements at the closest contact have been evaluated from the experimental data, that is, $V_0^T = 5118$ $cm^{-1}$ for the charge recombination to the triplet state and $V_0^G = 2670$ $cm^{-1}$ for that to the ground state. This indicates that the interfacial charge recombination in ATRA−$TiO_2$ is strongly coupled. The electronic coupling matrix element decays over the charge separation distance. In the microsecond time domain, the electronic coupling matrix element for the charge recombination to the triplet state decays to a value of 3.6 $cm^{-1}$, corresponding to the trapped electron located on the $TiO_2$ surface away from the adsorbates at a distance of 2.0 nm. The implication of this work to the EL device has also been discussed, which reveals that the fluorescence efficiency in a weakly coupled system can break the limit (25%) imposed by the spin statistics under certain conditions.

**Acknowledgment.** We thank Prof. J. P. Zhang for his suggestions in compiling software regarding SVD and global fitting. This work is supported by the National "Hundreds Talent Program" and National Fund for Key Basic Research under Grant No. G1998010102.

## References and Notes


(1) Levanon, H.; Norris, J. R. *Chem. Rev.* **1978**, *78*, 185−198.
(2) Frank, H. A.; Mclean, M. B.; Sauer, K. *Proc. Natl. Acad. Sci. U.S.A.* **1979**, *76*, 5124−5128.
(3) Lubitz, W.; Lendzian, F.; Bittl, R. *Acc. Chem. Res.* **2002**, *35*, 313−320.
(4) Shuvalov, V. A. *Biochim. Biophys. Acta* **1976**, *430*, 113−121.
(5) Thurnauer, M. C.; Katz, J. J.; Norris, J. R. *Proc. Natl. Acad. Sci. U.S.A.* **1975**, *72*, 3270−3274.
(6) Dutton, P. L.; Leigh, J. S.; Seibert, M. *Biochem. Biophys. Res. Commun.* **1972**, *46*, 406−413.
(7) Friend, R. H.; Gymer, R. W.; Holmes, A. B.; Burroughes, J. H.; Marks, R. N.; Taliani, C.; Bradley, D. C.; Dos Santos, D. A.; Brédas, J. L.; Lögdlund, M.; Salaneck, W. R. *Nature* **1999**, *397*, 121−127.
(8) Cao, Y.; Parker, I. D.; Yu, G.; Zhang, C.; Heeger, A. J. *Nature* **1999**, *397*, 414−417.
(9) Tang, C. W.; van Slyke, S. A. *Appl. Phys. Lett.* **1987**, *51*, 913−915.
(10) O'Regan, B.; Grätzel, M. *Nature* **1991**, *353*, 737−739.
(11) Hagfeldt, A.; Grätzel, M. *Acc. Chem. Res*. **2000**, *33*, 269.
(12) Siefermann-Harms, D. *Physiol. Plant.* **1987**, *69*, 561−568.
(13) Peterman, E. J. G.; Dukker, F. M.; van Grondelle, R.; van Amerongen, H. *Biophys. J.* **1995**, *69*, 2670−2678.
(14) Cogdell, R. J.; Frank, H. A. *Biochim. Biophys. Acta* **1987**, *895*, 63−79.
(15) Vlassiouk, I.; Smirnov, S.; Kutzki, O.; Wedel, M.; Montforts, F.-P. *J. Phys. Chem. B* **2002**, *106*, 8657−8666.
(16) Carbonera, D.; Di Valentin, M.; Corvaja, C.; Agostini, G.; Giacometti, G.; Liddell, P. A.; Kuciauskas, D.; Moore, A. L.; Moore, T. A.; Gust, D. *J. Am. Chem. Soc.* **1998**, *120*, 4398−4405.
(17) Hasharoni, K.; Levanon, H.; Greenfield, S. R.; Gosztola, D. J.; Svec, W. A.; Wasielewski, M. R. *J. Am. Chem. Soc.* **1995**, *117*, 8055−8056.
(18) Hasharoni, K.; Levanon, H.; Greenfield, S. R.; Gosztola, D. J.; Svec, W. A.; Wasielewski, M. R. *J. Am. Chem. Soc.* **1996**, *118*, 10228−10235.
(19) Wiederrecht, G. P.; Svec, W. A.; Wasielewski, M. R.; Galili, T.; Levanon, H. *J. Am. Chem. Soc.* **2000**, *122*, 9715−9722.
(20) Okada, T.; Karaki, I.; Matsuzawa, E.; Mataga, N.; Sakata, Y.; Misumi, S. *J. Phys. Chem.* **1981**, *85*, 3957−3960.
(21) Schulten, K.; Staerk, H.; Weller, A.; Werner, H.-J.; Nickel, B. *Z. Phys. Chem. (Frankfurt/Main)* **1976**, *101*, 371−390.
(22) Steiner, U. E.; Ulrich, T. *Chem. Rev.* **1989**, *89*, 51−147.
(23) Weng, Y. X.; Xu, J. Z.; Pan, J.; Lin, K. L.; Wang, L.; Yang, G. Z. *Acta Bot. Sin.* **2000**, *42*, 1215−1219.
(24) Weng, Y. X.; Li, L.; Liu, Y.; Wang, L.; Yang, G. Z.; Sheng, J. Q. *Chem. Phys. Lett.* **2002**, *355*, 294−300.
(25) Pan, J.; Benkö, G.; Xu, Y.; Pascher, T.; Sun, L.; Sundström, V.; Polívka, T. *J. Am. Chem. Soc.* **2002**, *124*, 13949−13957.
(26) Hubbard, R.; Kropf, A. *Proc. Natl. Acad. Sci. U.S.A.* **1958**, *44*, 130.
(27) Wald, G. *Science* **1968**, *162*, 230−239.
(28) Desilvestro, J.; Grätzel, M.; Kavan, L.; Moser, J. E.; Augustynski, J. *J. Am. Chem. Soc*. **1985**, *107*, 2988−2990.
(29) Vlachopoulos, N.; Liska, P.; Augustynski, J.; Grätzel, M. *J. Am. Chem. Soc.* **1988**, *110*, 1216−1220.
(30) Yamaguchi, S.; Hamaguchi, H. *J. Chem. Phys.* **1998**, *109*, 1397−1408.
(31) Chen, W. G.; Braiman, M. S. *Photochem. Photobiol.* **1991**, *54*, 905.
(32) Takeuchi, S.; Tahara, T. *J. Phys. Chem. A* **1997**, *101*, 3052−3060.
(33) Das, P. K.; Becker, R. S. *J. Am. Chem. Soc.* **1979**, *101*, 6348.
(34) Bobrowski, K.; Das, P. K. *J. Phys. Chem.* **1985**, *89*, 5079−5085.
(35) Merchán, M.; Gonzalez-Luque, R. *J. Chem. Phys.* **1997**, *106*, 1112−1122.
(36) Tavan, P.; Schulten, K. *J. Chem. Phys.* **1986**, *85*, 6602.
(37) Sashima, T.; Koyama, Y.; Yamada, T.; Hashimoto, H. *Chem. Phys. Lett.* **1999**, *299*, 187.
(38) Sashima, T.; Koyama, Y.; Yamada, T.; Hashimoto, H. *J. Phys. Chem. B* **2000**, *104*, 5011−5019.
(39) Koyama, Y.; Yamada, T.; Hashimoto, H. *J. Phys. Chem. B* **2000**, *104*, 5011−5019.
(40) Takemura, T.; Das, P. K.; Hug, G.; Becker, R. S. *J. Am. Chem. Soc.* **1978**, *100*, 2626.
(41) Drikos, G.; Rüppel, H. *Photochem. Photobiol.* **1984**, *40*, 85−91.
(42) Yamaguchi, S.; Hamaguchi, H. *J. Mol. Struct.* **1996**, *379*, 87.
(43) Sahyun, M. R. V.; Serpone, N. *J. Photochem. Photobiol. A: Chem.* **1998**, *115*, 231−238.
(44) Bondarev, S. L.; Tikhomirov, S. A.; Bachilo, S. M. *Proc. SPIE* **1990**, *497*, 1403.
(45) Drikos, G.; Rüppel, G. *Photochem. Photobiol.* **1984**, *40*, 93−104.
(46) Lo, K. K. N.; Land, E. J.; Truscott, T. G. *Photochem. Photobiol.* **1982**, *36*, 139−145.
(47) Ros, M.; Hogenboom, M. A.; Kok, P.; Groenen, E. J. J. *J. Phys. Chem.* **1992**, *96*, 2975.
(48) El-Sayed, M. A. *J. Chem. Phys*. **1962**, *36*, 573.
(49) El-Sayed, M. A. *J. Chem. Phys*. **1963**, *38*, 2834.
(50) Weng, Y. X.; Li, L.; Liu, Y.; Wang, L.; Yang, G. Z. *J. Phys. Chem. B* **2003**, *107*, 4356.
(51) Ellingson, R. J.; Asbury, J. B.; Ferrere, S.; Ghosh, H. N.; Sprague, J. R.; Lian, T.; Nozik, A. J. *J. Phys. Chem. B* **1998**, *102*, 6455−6458.
(52) Asbury, J. B.; Hao, E.; Wang, Y.; Ghosh, H. N.; Lian, T. *J. Phys. Chem. B* **2001**, *105*, 4545−4557.
(53) Benkö, G.; Kallioinen, J.; Korppi-Tommola, J. E. I.; Yartsev, A. P.; Sundström, V. *J. Am. Chem. Soc.* **2002**, *124*, 489−493.
(54) Khoudiakov, M.; Parise, A. R.; Brunschwig, B. S. *J. Am. Chem. Soc.* **2003**, *125*, 4637−4642.
(55) Weng, Y. X.; Wang, Y. Q.; Asbury, J. B.; Ghosh, H. N.; Lian, T. Q. *J. Phys. Chem. B* **2000**, *104*, 93−104.
(56) Ferrere, S.; Cregg, B. A. *J. Am. Chem. Soc*. **1998**, *120*, 843−844.
(57) Moser, J. E.; Gräzel, M. *Chimica* **1998**, *52*, 160−162.
(58) Robinson, G. W.; Frosch, R. P. *J. Chem. Phys*. **1963**, *387*, 1187.
(59) Wiederrecht, G. P.; Svec, W. A.; Wasielewski, M. R. *J. Am. Chem. Soc.* **1999**, *121*, 7726−7727.
(60) Colombo, D. P., Jr.; Bowman, R. M. *J. Phys. Chem.* **1996**, *100*, 18445−18449.
(61) Serpone, N.; Lawless, D.; Khairutdinov, R.; Pelizzetti, E. *J. Phys. Chem.* **1995**, *99*, 16655−16661.
(62) Marcus, R. A.; Sutin, N. *Biochim. Biophys. Acta* **1985**, *811*, 265.
(63) Moser, J.; Grätzel, M. *Chem Phys.* **1993**, *176*, 493−500.
(64) Gaal, D. A.; Hupp, T. J. *J. Am. Chem. Soc.* **2000**, *122*, 10956−10963.
(65) Lewis, N. S. *J. Phys. Chem. B* **1998**, *102*, 4843−4855.
(66) Mclendon, G.; Hake, R. *Chem. Rev*. **1992**, *92*, 481−490.
(67) Moser, C. C.; Keske, J. M.; Warncke, K.; Farid, R. S.; Dutton, P. L. *Nature* **1992**, *355*, 796−802.